Energy Reports 13 (2025) 5815–5827

Contents lists available at ScienceDirect

Energy Reports

journal homepage: www.elsevier.com/locate/egyr

Research Paper

Investigating CO_2 and hydrogen flow dynamics and efficiency optimization for underground storage and production: An experimental and simulation-based study

Apoorv Verma, Shankar Lal Dangi, Shruti Malik, Mayur Pal *

Department of Mathematical Modeling, Kaunas University of Technology, Kaunas 51368, Lithuania

ARTICLE INFO

Keywords:
Underground hydrogen storage and production
Experimental approach
Porous media
Simulation
Flow behavior
Sandbox
Optimization scenarios

ABSTRACT

This study uses an experimental and simulation-based approach to investigate hydrogen flow behavior and efficiency optimization during underground hydrogen storage and production (UHSP). Laboratory-scale sandbox experiments were conducted under low pressure to assess the dynamics of H_2, H_2, and CO_2 mixtures in porous sandstone media. The sandbox experiments revealed that sandstone formations, with high permeability, are effective for both H_2 and H_2 and CO_2 mixtures for gas storage, showing minimal leakage when combined with impermeable cap rocks, which were represented by a clay layer in the sandbox experiment. Further, a 2D mechanistic model was developed and simulated using tNavigator to validate the experimental results, simulating gas migration and reproducing the phenomenon seen in the sandbox modeling experiment. Subsequently, a scaleup study was also conducted, where various optimization scenarios were explored to enhance UHSP efficiency, which includes optimization based on injection duration, injection rates, and model heterogeneity.

1. Introduction

Hydrogen (H_2) potential as an alternative fuel was recognized several decades ago (Wallace and Ward, 1983). Excessive dependence on non-renewable sources such as fossil fuels, coal, and natural gas increases CO_2 emissions into the environment (Mubarak et al., 2024). The annual global average concentrations of CO_2 reached unprecedented levels of 414.7 ppm in 2021, which accounts for 74.4 % of total greenhouse gas (GHG) emissions (Akbar et al., 2024; Perone, 2024; Shang et al., 2024).Therefore, transitioning to sustainable and renewable energy sources is essential to achieving global net-zero emissions by 2050 (Renné, 2022). While options like solar, wind, and hydroelectric power are promising, they face supply fluctuations due to diurnal, seasonal, and climate changes (Ichimura and Kimura, 2019; Maghami et al., 2024). H_2 has become increasingly important as a clean energy carrier in achieving CO_2 neutrality. However, the challenge of large-scale H_2 storage is a significant barrier to advancing H_2 energy. Therefore, the present study addresses underground hydrogen storage and production (UHSP) aspects through mechanistic modeling and case optimization.

The geological formations like porous reservoirs, depleted oil and gas fields, saline aquifers, and salt caverns are suitable for UHSP (Hogeweg et al., 2022a,b; Indro et al., 2024; Thaysen et al., 2023; Vialle and Wolff-Boenisch, 2024). Dodangoda et al. (2024) noted that sandstone formations are suitable due to their high porosity, well-graded pore distribution, favorable pore connectivity, and minimal clay minerals and carbonates presence. Jahanbani Veshareh et al. (2022) reported that depleted hydrocarbon chalk reservoirs are technically suitable for H_2 storage, offering gas tightness with a leakage rate of 0.01 % per year. Moreover, a British company has stored H_2 (95 % H_2 and 3 %–4 % CO_2) at a depth of 400 m in salt caverns in Teesside, UK (Gielen et al., 2019), which confirms the feasibility of UHSP. Similarly, in Germany, the Kiel town gas project is a notable salt cavern H_2 storage facility with a capacity of 60 % (Liebscher et al., 2016). However, multiple risks are associated with UHSP, including chemical and biochemical reactions, H_2 loss and leakage, reservoir integrity, formation damage, geochemical reactions, and microbial activity (Maury Fernandez et al., 2024). For instance, Najafimarghmaleki and Dehghanpour (2024) reported that brine-rock interactions can cause the dissolution of halite, calcite (1.4 %-1.7 %), and dolomite (0.15 %-0.4 %), highlighting the importance of considering these effects in the safe design of underground energy storage.

Simulation studies can play a vital role in advancing the

* Corresponding author.
E-mail address: mayur.pal@ktu.lt (M. Pal).

https://doi.org/10.1016/j.egyr.2025.05.014
Received 31 January 2025; Received in revised form 29 April 2025; Accepted 8 May 2025
Available online 19 May 2025

understanding of UHSP. These studies provide critical insights into underground processes and reservoir behavior, including flow dynamics, storage capacity, interactions with reservoir rocks and fluids, etc.(Maury Fernandez et al., 2024; Shang et al., 2024). This can help optimize and successfully deploy UHSP, contributing to system performance and supporting the global energy transition. For instance, the storage efficiency attributed to H_2 reactions with rock skeletons and fluids leads to biological and nonbiological reactions (Wang, Wu, et al., 2023). The wettability of rocks in the H_2–fluids–rock system varies with formation conditions, impacting H_2 permeation ability. Moreover, variations in wettability caused by changes in temperature, pressure, and the presence of organic acid improve the dynamics of H_2 injection and withdrawal, optimizing the overall storage process (Iglauer et al., 2021). The interfacial tension between H_2 and brine is influenced by gas composition, with mixed gases like CH_4 and CO_2 reducing interfacial tension and improving injection and withdrawal efficiency (Dehghani et al., 2024).

While previously reviewed research (Berta et al., 2018; Tarkowski, 2019; Pan et al., 2021a,b; Zivar et al., 2021; Tarkowski and Uliasz-Misiak, 2022; Bahrami et al., 2023; Gomez Mendez et al., 2024; Verma et al., 2024; Verma et al., 2025) has demonstrated the feasibility of UHSP in geological formations such as porous reservoirs, salt caverns, and depleted hydrocarbon fields, significant gaps remain in understanding the complex subsurface processes that affect storage efficiency. Most studies are either simulation (Kolditz et al., 2012; Pfeiffer et al., 2017; Rahbari et al., 2019; Cai et al., 2022; Hogeweg et al., 2022a,b; Abdellatif et al., 2023) or pore-scale experimental studies (Lysyy et al., 2022; Boon and Hajibeygi, 2022; Gao et al., 2023; Jangda et al., 2023; Song et al., 2023; Wang, Yang, et al., 2023; Dokhon et al., 2024). However, numerical modeling and simulations can complement laboratory experiments to allow a greater range of research. Through an integrated study, many questions can be answered, including factors that affect reservoir and fluid properties within the storage zone and what happens when a gas mixture (H_2 and CO_2, in this study) is injected into the reservoir. No such studies are presented in the literature where both aspects are captured in an integrated manner. Additionally, the field of H_2 storage lacks any pilot demonstration, which poses challenges to understanding the flow behavior of H_2 in real geological formations (Verma et al., 2025). The study presented in this paper aims to bridge these gaps. It is essential to conduct integrated experimental and simulation studies to capture the dynamic interactions between hydrogen, reservoir rocks, and fluids under realistic storage and production conditions. This combined approach will enhance the accuracy of predictive models and provide actionable insights for optimizing H_2 injection, withdrawal, and overall storage efficiency.

Therefore, this study aims a) to analyze hydrogen flow behavior through experiment and simulation and b) to optimize efficiency using the simulation-optimization technique of various production-to-injection ratio scenarios. This study provides valuable insights into hydrogen flow behavior in porous media formation and optimization of hydrogen injection and production to identify the most efficient scenario. The findings can aid in designing more effective H_2 storage and production systems, ensuring that the full potential of hydrogen as a clean energy carrier is realized. The paper is organized as follows: 2 provides an overview of the governing flow equations for multiphase flow. 3 presents the material and methodology used to construct the experimental setup, corresponding simulation model, and optimization scenarios. 4 presents result and discusses results related to optimization scenarios. 5 presents some of this study's limitations. 6 presents conclusions.

2. Theory of governing equations

The present study uses the momentum equation that governs the flow of different phases (such as gas and water) within a porous medium. The equation is derived from Darcy's law and considers the pressure, viscosity, gravitational effects, and relative permeability of each phase (Whitaker, 1986; Dangi et al., 2023). The general form of the momentum equation is applied to both wetting and non-wetting phases, such as water (wetting phase) and CO_2 and H2 (non-wetting phase) in a typical reservoir system (Liu and Smirnov, 2008). The governing equation for each phase is expressed as:

$$\phi\frac{\partial S_\beta}{\partial t} + \nabla\cdot\{\frac{k_\beta}{\mu_\beta}\nabla(P_\beta+\rho_\beta gD)\} = Q_\beta \tag{1}$$

Where β represents a phase (e.g., gas, water, etc.), ϕ_β is the porosity of the medium for phase β, S_β is the saturation of phase β, k_β is the absolute permeability of the porous medium for phase β, μ_β is the dynamic viscosity of phase β, P is the pressure of phase β, ρ_β is the density of phase β, g is the gravitational acceleration, D is the vertical elevation (height), Q_β is the source term for phase β accounting for external fluxes like injection or production. Further, the finite volume method (FVM) solves the governing equation by discretizing the computational domain into small control volumes. This method is advantageous because it ensures mass conservation across control volume boundaries (Dangi et al., 2023). First, we express the equation in its integral form over a control volume Ω_i.We integrate the Eq. (1) over the control volume to get the Eq. (2).

$$\int_{\Omega_i}(\phi\frac{\partial S_\beta}{\partial t})dV+\int_{\Omega_i}\nabla\cdot\{\frac{k_\beta}{\mu_\beta}\nabla(P_\beta+\rho_\beta gD)\}dV=\int_{\Omega_i}Q_\beta dV \tag{2}$$

Now, applying the divergence theorem to the second term (the term involving the flux) in Eq. (2), the volume integral converted into a surface integral over the boundary $\partial\Omega_i$ of the control volume, as shown in Eq. (3).

$$\int_{\Omega_i}\nabla\cdot\{\frac{k_\beta}{\mu_\beta}\nabla(P_\beta+\rho_\beta gD)\}dV=\int_{\partial\Omega_i}\frac{k_\beta}{\mu_\beta}\{\nabla(P_\beta+\rho_\beta gD)\}\cdot ndA \tag{3}$$

Where, n is the outward-pointing unit normal vector on the surface of the control volume. Thus, the integral form of the governing equation has become Eq. (4).

$$\int_{\Omega_i}(\phi\frac{\partial S_\beta}{\partial t})dV+\int_{\partial\Omega_i}\frac{k_\beta}{\mu_\beta}\{\nabla(P_\beta+\rho_\beta gD)\}\cdot ndA=\int_{\Omega_i}Q_\beta dV \tag{4}$$

Next, the approximation of the integral is performed by discretizing the control volume Ω_i into smaller sub-volumes (often denoted as grid cells in numerical simulations). Volume integrals are estimated based on values at cell centers, and surface integrals (flow through control volume boundaries) are calculated based on values at cell mouths. The term $\frac{\partial S_\beta}{\partial t}$ in Eq. 4 is the mass accumulation term. Now, this term is discretized using a forward Euler method (Yang et al., 2018) for the time derivative shown in Eq. (5).

$$\frac{\partial S_\beta}{\partial t} \approx \frac{S_\beta^{n+1}-S_\beta^n}{\Delta t} \tag{5}$$

Where, S_β^n is the saturation of phase β at the previous time step, and S_β^{n+1} is the saturation at the current time step. Now, the pressure gradient term is discretized over the boundary of the control volume i.e., $\partial\Omega_i$ shown in Eq. (6).

$$\int_{\partial\Omega_i}\frac{k_\beta}{\mu_\beta}\{\nabla(P_\beta+\rho_\beta gD)\}\cdot ndA \approx \sum_{f\in\partial\Omega_i}\frac{k_\beta}{\mu_\beta}\cdot\frac{P_\beta^f-P_\beta^i}{\Delta x_f}A_f \tag{6}$$

Where, $P_\beta^f and P_\beta^i$ are the pressures at the face f and the center of control volume i, respectively, Δx_f is the distance between the cell centers along the face f, A_f is the area of the face f (the surface area of the control volume face). Now, the source term Q_β Eq. (4) is discretized, as shown in Eq. (7). This equation represents the total injection or production rate within the control volume.

$$\int_{\Omega_i} Q_\beta dV = Q_\beta \Delta V_i \tag{7}$$

Combining all the terms of Eqs. (5), (6), and (7), the discretized form of the Eq. (4) for each control volume i becomes Eq. (8).

$$\phi \frac{S_\beta^{n+1} - S_\beta^n}{\Delta t} \Delta V_i + \sum_{f \in \partial\Omega_i} \frac{k_\beta}{\mu_\beta} \cdot \frac{p_\beta^f - p_\beta^i}{\Delta x_f} A_f = Q_\beta \Delta V_i \tag{8}$$

Finally, Eq. (8) is used to solve the problems in fluid flow in porous media, which is based on FVM. Furthermore, a compositional model is utilized for the study to simulate the thermodynamic behavior of reservoir fluids consisting of CO_2 and H_2. The behavior of these components is modelled using the Peng-Robinson (PR) equation of state (EOS) (Peng and Robinson, 1976), which is shown as Eq. (9).

$$P = \frac{RT}{v - b} - \frac{a}{(v + m_1 b)(v + m_2 b)} \tag{9}$$

Where the values of m_1 *and* m_2 *are* $1 + \sqrt{2}$ and $1 - \sqrt{2}$, respectively, P is the pressure, T is the temperature, v is the molar volume of the mixture, and a and b are parameters that depend on its critical properties.

3. Material and methodology

The methodology to explore the H_2 flow behavior and storage feasibility has been divided into three parts: a) experimental work, b) simulation work, and c) optimization scenarios. The experimental setup was primarily designed to study the CO_2 and H_2+CO_2 injection and migration behavior in porous media under controlled conditions. Further, a 2D mechanistic model was developed using tNavigator to simulate the flow pattern in layered geological formations to verify the experiment result. Next, various optimization scenarios were studied, using cyclic injection and production strategies to enhance UHSP efficiency.

3.1. Experimental design and execution

An experimental setup (sandbox model) was designed to study CO_2 and H_2+ CO_2 migration behavior in porous media on a laboratory scale, schematic layout is presented in Fig. 1a, and the actual tank setup is shown in Fig. 1b. The tank was 15 × 15 × 5 in. in size, made of a 20 mm thick acrylic sheet, which allowed visual monitoring of internal conditions, and was airtight with a limit of low-pressure resistance to up to 1 bar, as shown in Fig. 1b. The top and bottom of the tank were made from stainless steel because of its high tensile strength and durability under pressure. The tank was equipped with pressure and temperature monitoring sensors for data collection. A valve was installed at the top of the tank to collect the sample and identify the leakage. An injection port was provided to inject the gas and dye. Further, to mimic the subsurface conditions in a layered form, we utilized a combination of materials with varying grades and properties, including fine sand, sandstone, clay, and gravel (pressure up to 1 bar). Detailed characteristics of materials used in layered formation inside the tank before CO_2 and H_2 + CO_2 injection are listed in Table 1. Bromothymol blue (BTB), a pH-sensitive dye (sourced from Thomas Baker), was used to saturate the tank media thoroughly and further to observe the movement and trapping of gas inside the tank (Chauhan, 2018; Smith et al., 2020). The experimental procedure comprised four steps: (1) material filling and compaction to create heterogeneous geological formation of different grade material, (2) saturating the media with brine and BTB dye to replicate subsurface conditions, (3) gas injection phase, (4) data collection. The tank was cleaned after each experiment to prevent contamination before the following experiment. Fig. 1a illustrates a schematic design of an experimental tank setup, while Fig. 1b depicts the actual tank setup filled with varying permeability material.

3.2. Sandbox simulation model

A 2D mechanistic model was developed, replicating the sandbox model using tNavigator (version 24.2). The model is not a replica but a close representation of the sandbox experimental setup. Further, the simulation model consists of five flow units. Each geological layer was assigned a specific material type, as listed in Table 2, and grid properties used in the present numerical simulation model are listed in Table 3. The model represents gravel as a top layer, followed by a clay layer with a permeability of 0.0005 mD, a fine sand layer with a permeability of 30.87 mD, a sandstone layer with a permeability of 83.08 mD, a final fine sand layer, from top to bottom sequence, shown in Fig. 2a and

Table 1
Detailed characteristics of materials used in layer formation inside the tank.

Material	Porosity (in percentage)	Permeability (Darcy)	Grain size (mm)	Avg. grain size (mm)
Sand	39	3087	0.5	0.5
Sandstone	41	8308	0.8	0.8
Clay	48	492	0.18	0.18
Gravel	46	524357	5–7	6

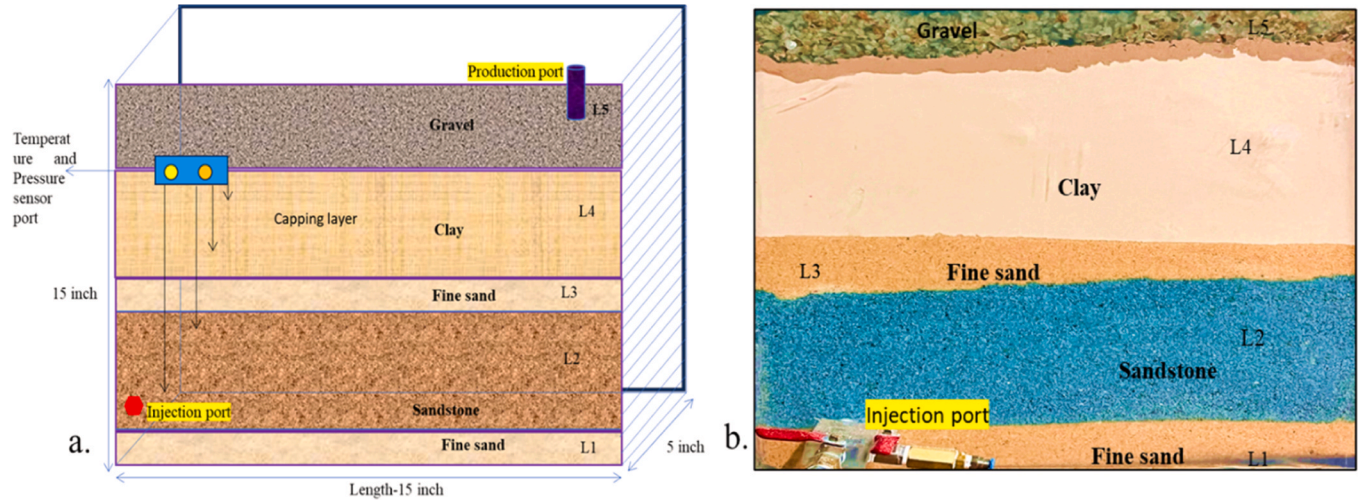

Fig. 1. Experimental tank setup a) schematic layout b) actual tank setup filled with varying permeability material.

Table 2
Properties used in the present numerical simulation model.

Layer	Thickness (inch)	Porosity (%)	Permeability (mD)
A (Gravel)	2	46	5243.57
B (Clay)	5	.05	.0005
C (Fine Sand)	1	39	30.87
D (Sandstone)	6	41	83.08
C (Fine Sand)	1	39	30.87

Table 3
Grid properties used in the present numerical simulation model.

Parameters	Dx (m)	Dy (m)	Dz (m)	Nx	Ny	Nz
Values	0.01	0.127	0.0254	100	1	15

boundary condition in Fig. 2b, see Table 2 for flow unit porosity and permeability. The simulation model has 100 cells in the x-direction, 15 in the z-direction, and 1 in the y-direction, see Table 3. The model aims to replicate H_2 flow behavior to validate the experimental study. The model has no-flow boundary conditions on all sides, with source and sink conditions at the bottom and top of the model, see Fig. 2b. The source and sink are represented by two wells: one for injection and one for production. Injection of H_2 and CO_2 is through the 13th layer, and production was from the top layer to replicate if there is any leakage from the cap rock. The reservoir's initial H_2 and CO_2 saturation are kept at zero, and the model is initially fully saturated with brine. After that, the flow behavior was observed when only CO_2 was injected and when a mixture of H_2 and CO_2 was injected.

3.3. Optimization study

The experimental and simulation models described in Sections 3.1 and 3.2 represent small-scale setups. Scaling up the results is necessary for the practical application of the findings obtained from experimental and simulation models. Therefore, a scaleup study was conducted using a mechanistic subsurface model. The objective of the scaleup study was to investigate the H_2 storage efficiency, which was analyzed with the help of an injection production parameter optimization. For the optimization study, a preliminary survey was conducted to collect the baseline data of the Syderiai deep saline aquifer, which was investigated earlier as a potential CO_2 and natural gas storage site in the Lithuania Baltic basin (Malik et al., 2024). The Baltic basin consists of a Cambrian sandstone reservoir, sealed by carbonaceous-shaly caprocks, and characterized by the sandstone lithology of the Deimena formation of the Middle Cambrian age (Malik et al., 2024). The depth of the saline reservoir ranges from 0.3 km to over 2 km. It is one of Lithuania's most significant deep saline aquifers, covering an area of 26 km^2 with a thickness of 57 m and a top depth of 1458 m. The aquifer has a porosity of 16 %, a permeability of 400 mD, and a net-to-gross value (NTG) of 0.75 (Malik et al., 2023). These reservoir properties have been used as input data to design a 3D mechanistic model using average properties for simulating various optimization scenarios. Fig. 3 shows how the optimization study was organized. A 3D mechanistic model was developed using tNavigator (version 24.2) to evaluate the feasibility of UHSP in the Syderiai deep saline aquifer. For the optimization study, two cases were designed: a) a homogenous model having averaged porosity and permeability values representing Syderiai deep saline aquifer and b) a heterogenous model to mimic reservoir conditions; the model incorporates spatially varying permeability and porosity in the x, y, and z directions (Fig. 4) but still using same Syderiai model properties as basis. In the homogeneous case, we assumed the same porosity and permeability for all reservoirs. In the heterogeneous case, a few variations were used. In the first heterogeneous 10 % variance on permeability and porosity was assumed from the base values. In the second heterogeneous case, an additional 20 % variance in porosity and permeability was assumed compared to the base case. And in the third heterogeneous case, an additional 40 % variance in porosity and permeability was assumed compared to the base case.

Further, in the homogenous model, two cases (cases A and B) were initially considered with differences in the layer of production. Both cases were designed to identify the most efficient injection rate. The case

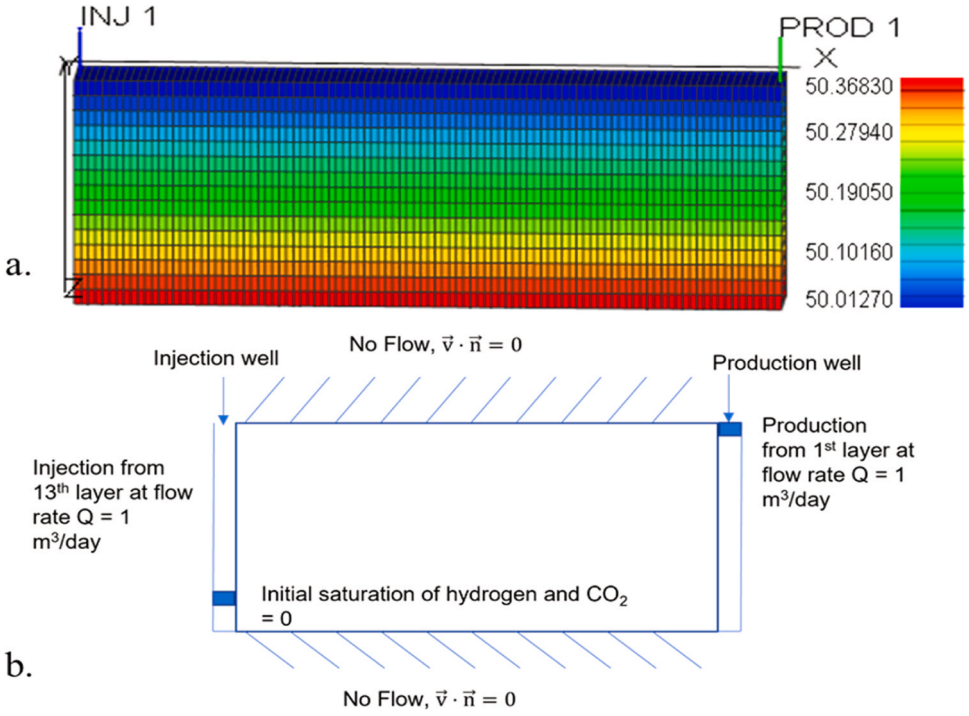

Fig. 2. Sandbox simulation model a) layered model configuration: gravel, clay, fine sand, and sandstone with permeability variations b) boundary condition applied in the simulation to replicate the laboratory test.

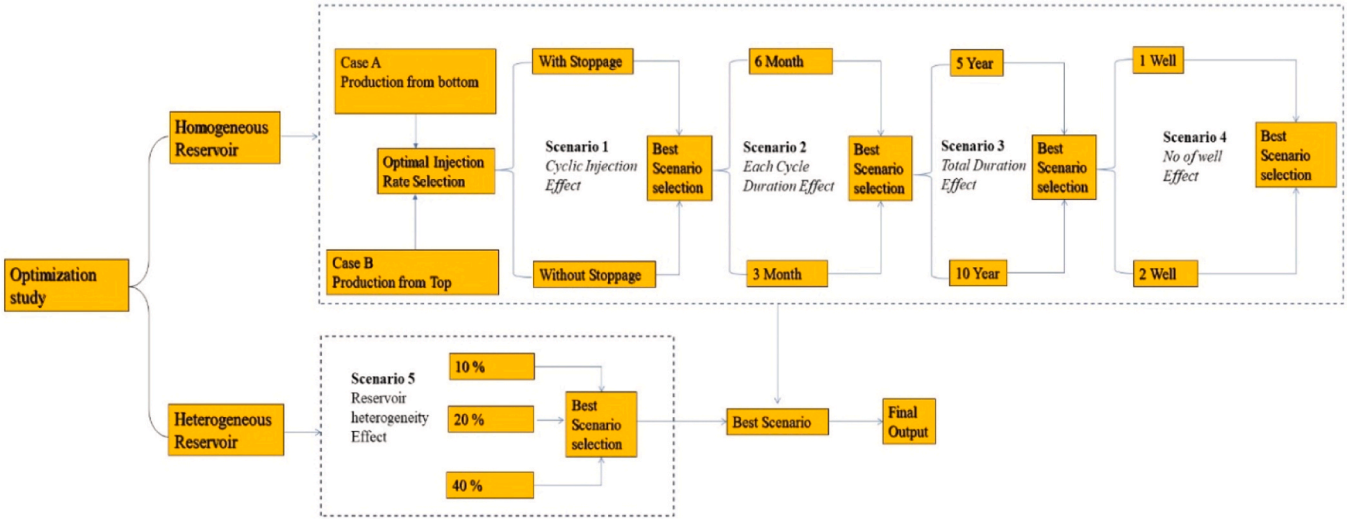

Fig. 3. Comprehensive workflow design to streamline the steps involved in optimization.

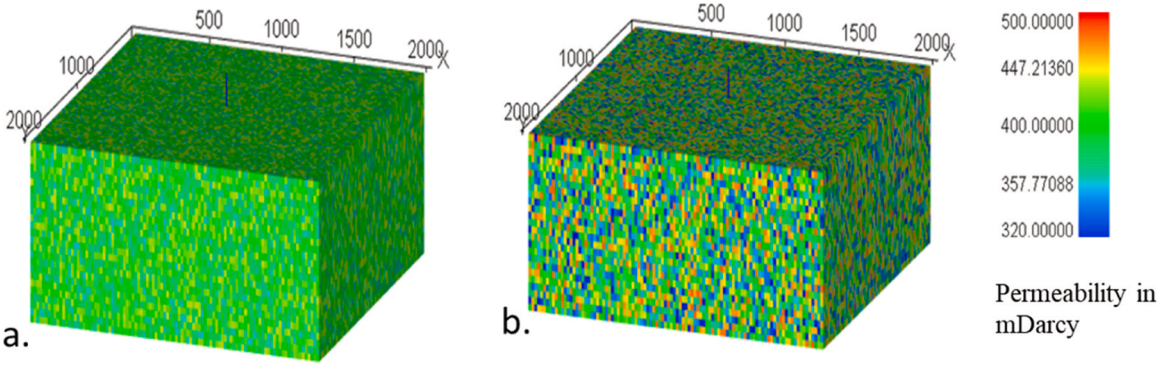

Fig. 4. Heterogeneous reservoir models (a) 10 % of heterogeneity permeability and (b) 20 % of heterogeneity permeability.

with better efficiency was taken for further optimization scenarios. In Table 4, Dx, Dy, and Dz are the model's dimensions (in meters) in the x, y, and z directions, respectively. Likewise, Nx, Ny, and Nz are the number of grids in the x, y, and z directions, respectively. BHP_{Inj} and BHP_{pro} are the borehole injection and production pressure (in bar). Methane (CH_4) was used as a cushion gas in the present simulation (Izadi Amiri et al., 2024; Saeed and Jadhawar, 2024).

4. Results and discussion

4.1. Experimental results

The experiments were successfully executed with CO_2 and $H_2 + CO_2$ injections into sandstone media, aiming to understand the flow behavior under controlled subsurface conditions. Findings suggest that after injecting CO_2, the reaction between CO_2 and water formed carbonic acid (H_2CO_3), leading to pH shifts that altered BTB's color from blue in alkaline conditions (pH > 7.6) to yellow in acidic conditions (pH < 6.0), effectively indicating gas migration. Moreover, the dissolution of CO_2 in brine causes a local decrease in pH, observed by color change in the dye. The yellow color from the blue dye indicated acidic conditions, confirming the dissolution of CO_2. Furthermore, increasing the CO_2 injection pressure displaced the brine-dye mixture within the sandstone media. The gas migration due to the dye was tracked visually, and breakthrough points were identified, presented in Fig. 5. The observations revealed preferential flow paths where CO_2 displaces brine, particularly in the high-permeability layer (sandstone). Furthermore, in this case, the layer interfaces acted as partial barriers, leading to localized trapping of CO_2 or slower displacement rates in the low-permeability layers, as seen in Fig. 5b and c. Over time, as the brine was displaced, the porous sandstone layer became progressively saturated with CO_2. Capillary forces in the smaller pores trapped the residual brine, while the larger pores allowed CO_2 to migrate more freely. This led to stable CO_2 bubbles or pockets within the brine-saturated media (Fig. 5b). On the contrary, some leakage was observed at the top layer of the setup, which may have been due to the expansion of the tank. The trapped gas (between the sandstone and clay layer) was noticed to move upwards slowly. However, the chances of leakage/upward movement would have decreased if the gas were utterly dissolved in the brine solution. However, the main reason for the leakage could be increased pressure inside the tank.

Furthermore, the layered formation was recreated for H_2+CO_2

Table 4
Properties used in the numerical simulation model.

Parameters	Dx(m)	Dy(m)	Dz(m)	Nx	Ny	Nz	BHP_{Inj}(bar)	BHP_{pro}(bar)
Values	20	20	2.28	100	100	25	150	50

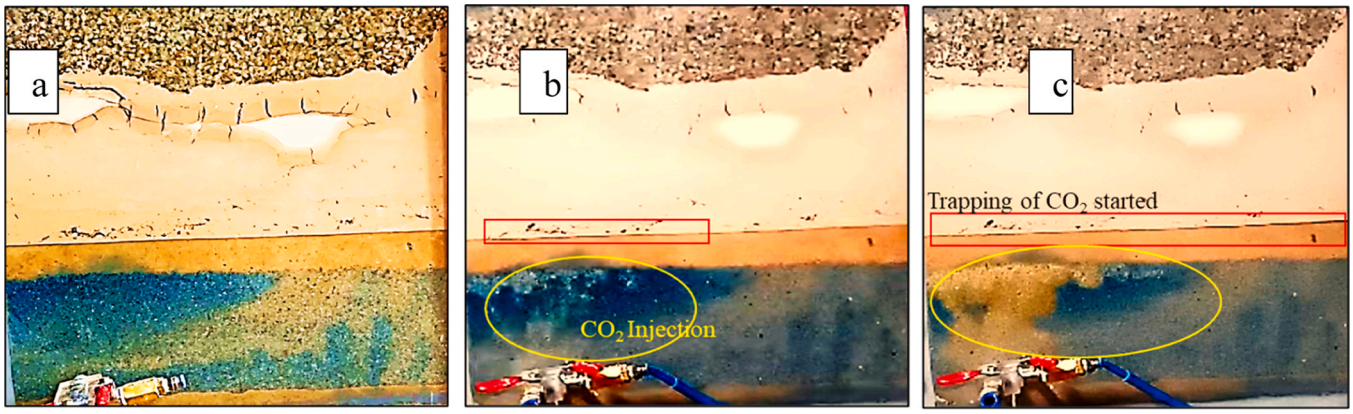

Fig. 5. CO_2 injection stages a) initial injection at t = 0, pressure (p) = 0, b) at t = 1 min, pressure (p) = 0.5 bars c) at t = 4.50 min, pressure (p) = 0.910 bars.

mixture injection to see the behavior of H_2 in porous media storage. The tank's base consisted of a 1-inch layer of fine sand, selected for its high permeability to support uniform gas flow. Above this, a 5–6-inch sandstone layer was added, with varying thicknesses for different cases to analyze gas migration and storage. In this case, the sandstone layer was thickened to better mimic natural geological formations and to observe how the gas mixture (H_2+CO_2) behaves in a more extensive porous medium. On top of the sandstone, another 1-inch fine sand was used as a transition layer, enhancing gas flow, and stabilizing the setup. A 5–6-inch-thick layer of clay was placed above the fine sand, acting as an impermeable cap rock to prevent gas from migrating upward, mimicking natural containment mechanisms. A gravel layer was added at the top to mimic the pressure exerted by overlying geological formations. Finally, the tank was tightly sealed (up to 1 bar) with a steel cover, secured by bolts, ensuring the system could withstand the high pressures associated with gas mixture injection.

The visual observations are presented in Figs. 6 and 7 for both phases: a) injection and b) trapping phase and development of fracture/fault, respectively. The movement of H_2+CO_2 through the sandstone media was observed from left to right, showing that the porous structure of the sandstone facilitated gas migration. This confirmed that sandstone is a permeable medium, allowing gases to flow through its interconnected pores. The gases were trapped in the center of the tank, just below the clay layer. This behavior indicated that while sandstone allows gas flow, it relies on an overlying impermeable layer (such as clay) to trap the gases and prevent further vertical movement. This demonstrated the effectiveness of porous sandstone media for storing gases when combined with a sealing layer. As gas injection continued, pressure gradually built up within the tank, reaching a maximum of 0.49 bar. At this point, the porous sandstone media retained the gas without showing signs of leakage through the layered formation. When the system pressure exceeded 0.49 bar, the tank expanded, and leakage occurred. However, the leakage was not through the sandstone or clay but rather from the top layer of the system, indicating that while the sandstone media could handle pressure up to a certain point, the structural containment of the system was compromised. Notably, the clay layer, acting as a cap rock, did not fracture under increased pressure. This behavior suggests that the sandstone below can store gases effectively if paired with an impermeable layer like clay, which prevents vertical gas escape and ensures containment within the storage formation.

4.2. Simulation outcomes

The simulation results highlight the dynamic movement and saturation profiles of CO_2 in a porous medium. Fig. 8a-f shows the saturation profiles of CO_2 movement in the porous medium at various time intervals. As the pressure gradient primarily drives migration, the result shows that CO_2 stays concentrated close to the injection well (INJ 1) during the initial injection phase (t = 35 sec. to t = 5 min 11 sec.), generating a confined plume. As CO_2 displaces fluids, intermediate saturation zones (green and yellow) emerge as the gas expands laterally and vertically during the plume growth phase (t = 10 min to t = 30 min). At this stage, CO_2 migrates upward because of its lower density, indicating the dominance of advection-driven flow and the formation of gravity segregation. Between t = 35 and t = 90 minutes, during the saturation and stability phase, the plume expansion rate slowed as the pressure gradient decreased, attributed to diffusion, making the saturation profile smoother. The extended high saturation region (red) near the injection well suggests practical storage and the

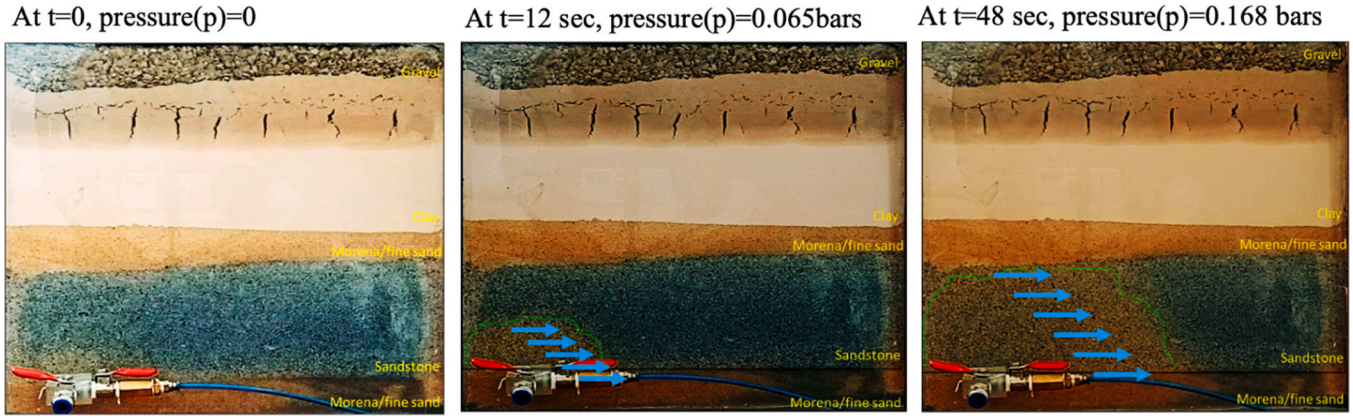

Fig. 6. Visualization of gas mixture during initial injection phase (1:1 Ratio) and migration across sandstone layer over the time and pressure intervals.

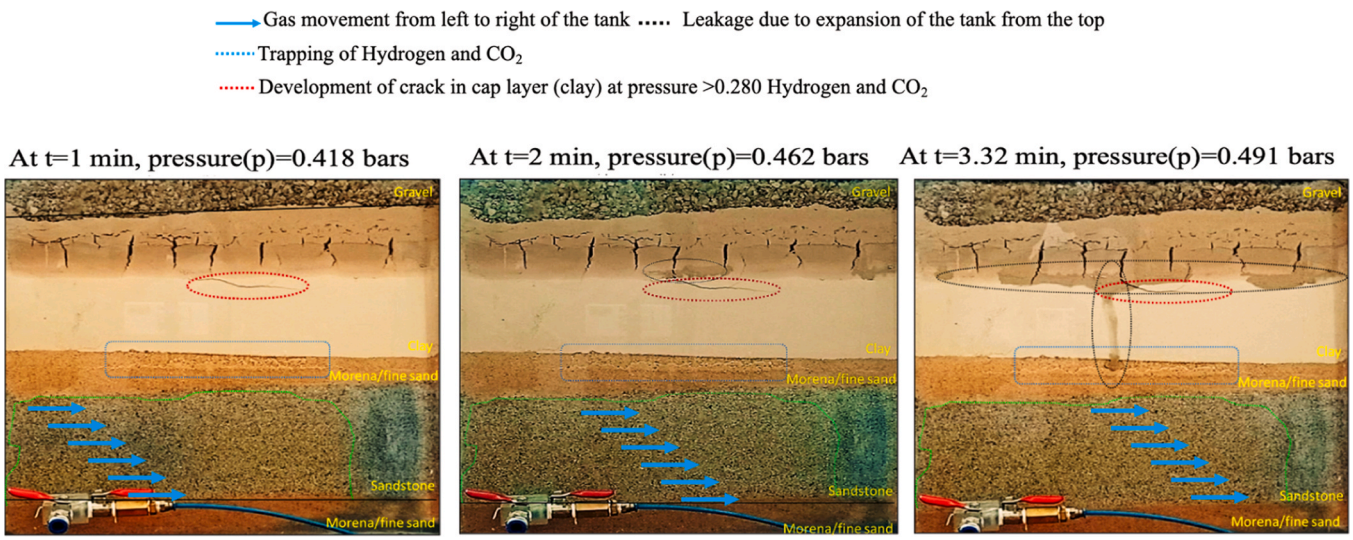

Fig. 7. Trapping phase and development of fracture/fault over the time and pressure intervals.

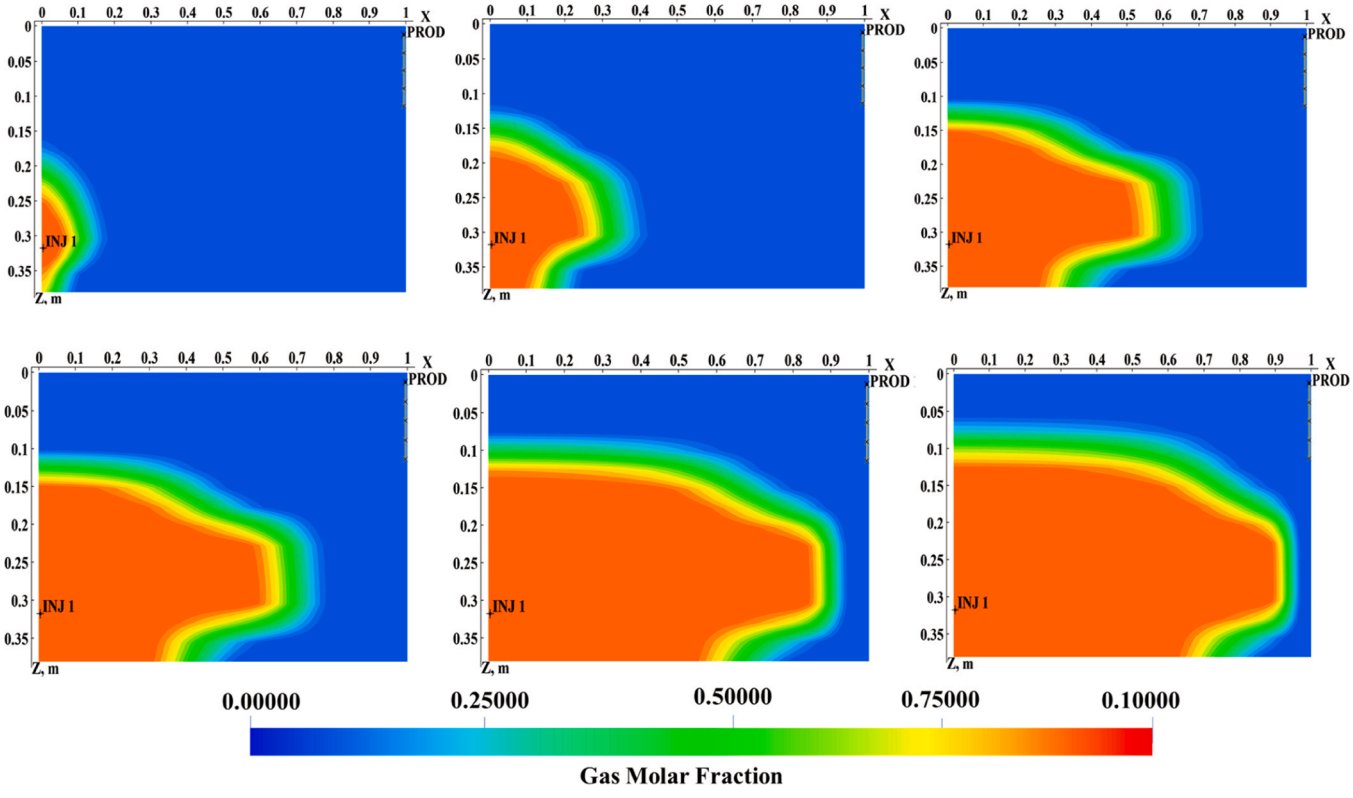

Fig. 8. Saturation profiles of CO_2 migration in porous media over different time intervals (a-f).

gradual transition indicates displacement processes. Further, Fig. 9a to f shows the dynamic saturation profiles of CO_2+H_2 in a porous material from 35 seconds to 90 minutes. Initially, there is a localized saturation gradient (red and yellow close to the injection point) and a concentration of gases close to the point. The mixture of gases moves toward the right-hand side. Over time, migration indicates a similar distribution of gas mixture as CO_2 saturation profiles.

Fig. 10 shows the gas-in-place distribution (in tons) over time for CO_2 injection and CO_2+H_2 injection at 50 % proportions, illustrating distinct flow behavior at different time intervals. Initially, the migration of CO_2+H_2 and CO_2 was similar. CO_2 injection exhibits a more concentrated gas distribution near the injection well (INJ 1). At the same time, the CO_2 + H_2 mixture achieves a broader and more uniform distribution, which might be due to the lower density and higher mobility of H_2 (Schlapbach, 2002). Over time, CO_2 shows localized accumulation, whereas the CO_2 + H_2 mixture diffuses more effectively toward the production well (PROD), indicating improved displacement efficiency. Quantitatively, the CO_2 + H_2 scenario demonstrates slightly lower gas-in-place values due to H_2's lower mass density, suggesting that incorporating hydrogen alters the flow behavior during storage. Moreover, gas migration in place is identical when analyzing the saturation profile of CO_2 (Fig. 8) and CO_2+H_2 mix (Fig. 9). However, the front of the CO_2+H_2 gases migrates more than CO_2 after some time due to CO_2 dissolution. Also, from Fig. 10, the amount of CO_2 as gas in place is more

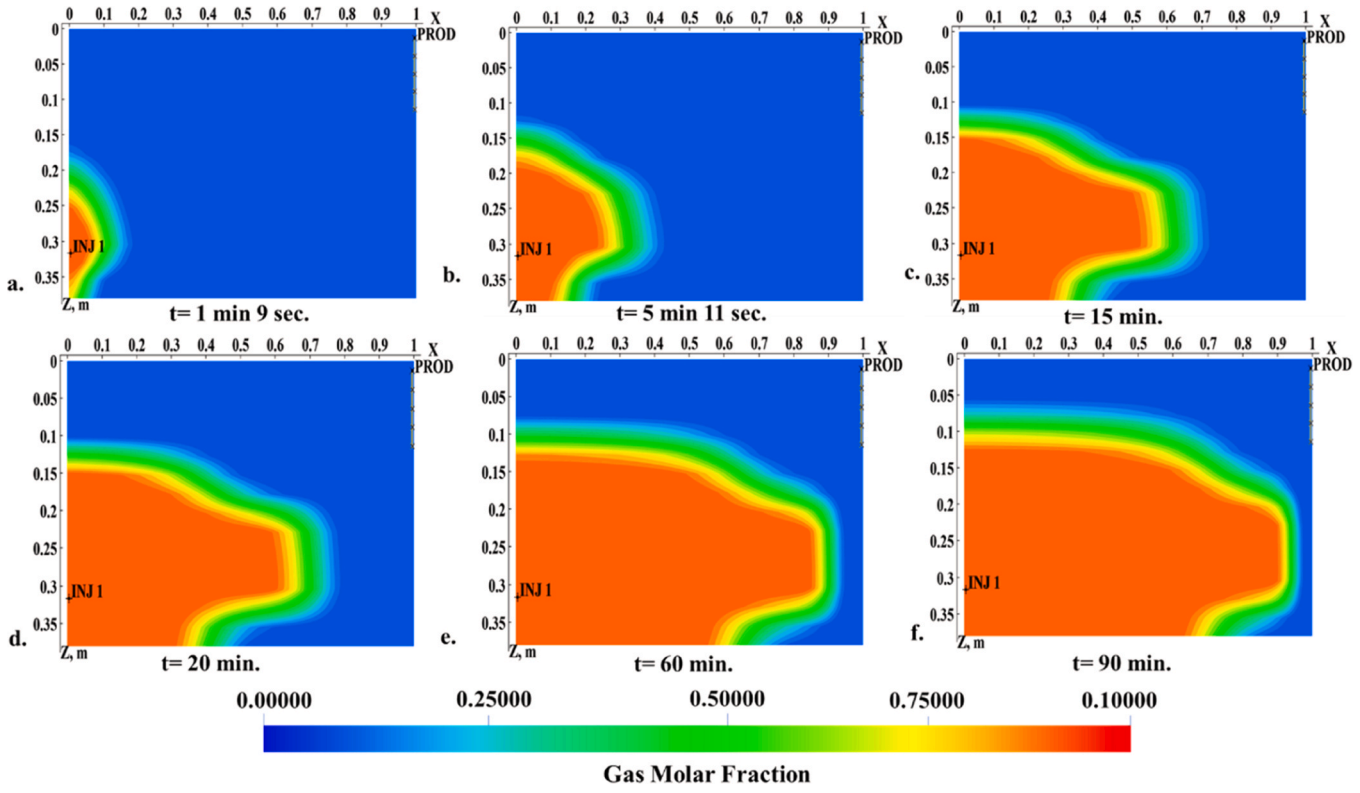

Fig. 9. Saturation profiles of CO_2+H_2 in porous media over different time intervals (a-f).

than that of the CO_2+H_2 mixture. Before 30 minutes, the migration of CO_2+H_2 seems to grow towards the production point (PROD), while the movement of CO_2 has not been observed towards the production point (PROD).

4.3. Optimization strategies

Initially, two homogenous cases (A and B) were designed to identify the best injection rate for further optimization scenarios. The results for each case are shown in Fig. 11a and b. In case A, H_2 was injected into the bottom layer for 6 months, followed by a 6-month production period from the same layer, and this cycle was repeated over 10 years. The efficiency improved as the injection volume increased, with an injection rate of 1.4 mln. Sm^3 /day achieved the highest efficiency (0.8243) and an injection rate of 0.2 mln. Sm^3 /day yielding the lowest efficiency (0.4819). This indicates that larger H_2 injection volumes lead to more effective utilization. Additionally, water production was higher at 1.4 mln. Sm^3 /day injection rate, producing 4800.69 th. Sm^3 water, compared to the 0.2 mln. Sm^3 /day case, which resulted in the lowest water production at 3396.84 th. Sm^3 . Further, in case B, H_2 was still injected into the bottom layer, but production occurred from the top layer. Furthermore, gas losses in Case B were significantly lower, ranging from 79.96 to 273.25 mln. Sm^3 , compared to 189.62–384.58 mln. Sm^3 in Case A. Additionally, comparing loss percentages in both cases suggests that Case B consistently achieved lower loss percentages than Case A (Fig. 12a). The analysis suggests that Case B consistently outperformed Case A in efficiency in terms of gas loss. However, efficiency improved with increasing injection rates in both cases. Still, Case B achieved higher values (e.g., 0.866 at 1.2 Sm^3/day vs. 0.815 in Case A) while maintaining lower loss percentages (e.g., 0.134 vs. 0.185). Moreover, water production in Case B was reduced across all injection rates, with 3523.32 th. Sm^3 at 1.2 Sm^3 /day compared to 4685.41 th. Sm^3 in Case A. In case B, water production volume suggests that the top layer produces less water than case A, making it a better option for H_2 injection efficiency (Fig. 12b). Additionally, increasing the injection rate from 1.2 mln. Sm^3 /day to 1.4 mln. Sm^3 /day did not significantly improve efficiency and increased water production. This suggests that an injection rate of 1.2 mln. Sm^3 /day in Case B provides optimal performance with high efficiency, minimal gas loss, and lower water production. Based on this, it was decided to optimize efficiency, keeping an injection rate of 1.2 mln. Sm^3 /day for further scenarios.

4.3.1. Scenario 1: cyclic injection with and without stoppage

This scenario evaluates the impact of a 4-month injection phase followed by a 2-month stoppage and 6 months of production at an injection rate of 1.2 mln. Sm^3 /day. The "without stoppage" case outperformed the "with stoppage" scenario, achieving higher injection and production volumes (1887.11 mln. Sm^3 and 1633.52 mln. Sm^3, respectively) compared to 1352.54 mln. Sm^3 and 1162.35 mln. Sm^3 . Efficiency was slightly better without stoppage (86.6 % vs. 85.9 %), despite higher absolute losses (253.59 mln. Sm^3 vs. 190.19 mln. Sm^3) but with a lower loss percentage (13.44 % vs. 14.06 %). However, water production was higher without stoppage (3523.32 th. Sm^3 vs. 3371 th. Sm^3). Consequently, the "without stoppage" scenario was selected for further optimization.

4.3.2. Scenario 2: 3-month and 6-month injection and production cycle

The 3-month cycle outperformed the 6-month cycle, achieving higher injection (2128.46 mln. Sm^3 vs. 1887.11 mln. Sm^3) and production volumes (1872.11 mln. Sm^3 vs. 1633.52 mln. Sm^3). Efficiency was also improved in the 3-month cycle (88 % vs. 86.6 %), with a reduced loss percentage (12 % vs. 13.4 %) compared to the 6-month cycle. Although losses were similar in absolute terms (~256 mln. Sm^3), the shorter cycle demonstrated a lower water production volume (3495 th. Sm^3 vs. 3523.32 th. Sm^3). This suggests that shorter cycles enhance efficiency and reduce water production. Fig. 13 illustrates pressure variations for the two cycles, showing more frequent pressure drops in the 3-month cycle, which may accelerate operational stress. Next, scenario 3 was studied to observe the efficiency by reducing the observation period from 10 years to 5 years while maintaining the 3-

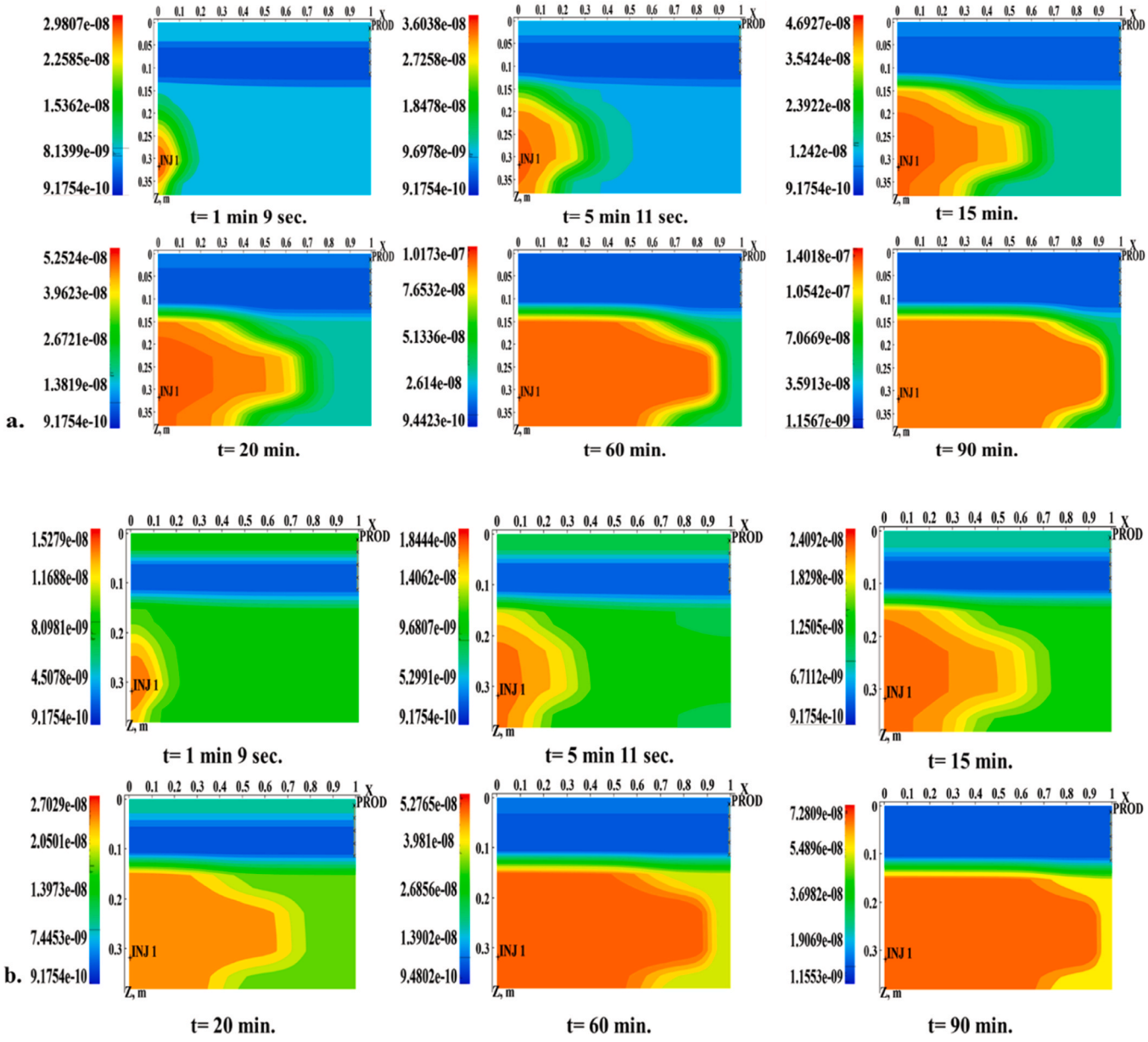

Fig. 10. Visual comparison of gas in place (Mass, Tons) at different time intervals for CO_2 injection and CO_2+H_2 injection.

month injection and production cycle.

4.3.3. Scenario 3: Reducing the observation period from 10 to 5 years

Reducing the observation period from 10 years to 5 years resulted in a lower injection volume (1030.46 mln. Sm^3) and production volume (880.28 mln. Sm^3) compared to the 10-year scenario (2128.46 mln. Sm^3 and 1872.11 mln. Sm^3). Efficiency also declined from 88 % to 85.4 %, while the loss percentage increased from 12 % to 18.4 %. Additionally, water production was significantly higher in the 5 years (5206.02 th. Sm^3 vs. 3495 th. Sm^3). These results indicate that a longer observation period enhances efficiency, reduces losses, and minimizes water production, making it the preferred option for optimizing gas recovery. Next, it was decided to investigate efficiency improvements with multiple wells for injection and production in Scenario 4.

4.3.4. Scenario 4: Using multiple wells for injection and production

A comparison of single- and two-well configurations (200 m apart) revealed that the single-well setup offered higher efficiency (88 % vs 86.3 %) and lower loss (256.35 mln. Sm^3 vs. 293.18 mln. Sm^3). Water production was also lower in the single-well scenario (3495 th. Sm^3 vs. 4078.91 th. Sm^3). Although the two-well setup increased injection capacity (2134.25 mln. Sm^3 vs. 2128.46 mln. Sm^3), the single-well configuration proved more effective overall, with reduced losses and water production. Finally, scenario 5 explored how the performance changes when the formation is heterogeneous.

4.3.5. Scenario 5: Impact of reservoir heterogeneity

Increasing reservoir heterogeneity enhanced storage efficiency and reduced water production. A 40 % heterogeneous formation paired with a 3-month injection cycle achieved the highest efficiency (88.2 %), the lowest loss percentage (11.8 %), and reduced water production (3215.9 th. Sm^3). Fig. 14 illustrates that efficiency improved incrementally with heterogeneity levels: from 86.6 % in homogeneous formations to 87.1 % with 40 % heterogeneity. This trend highlights the potential of moderate heterogeneity in optimizing flow paths and gas distribution for better hydrogen storage.

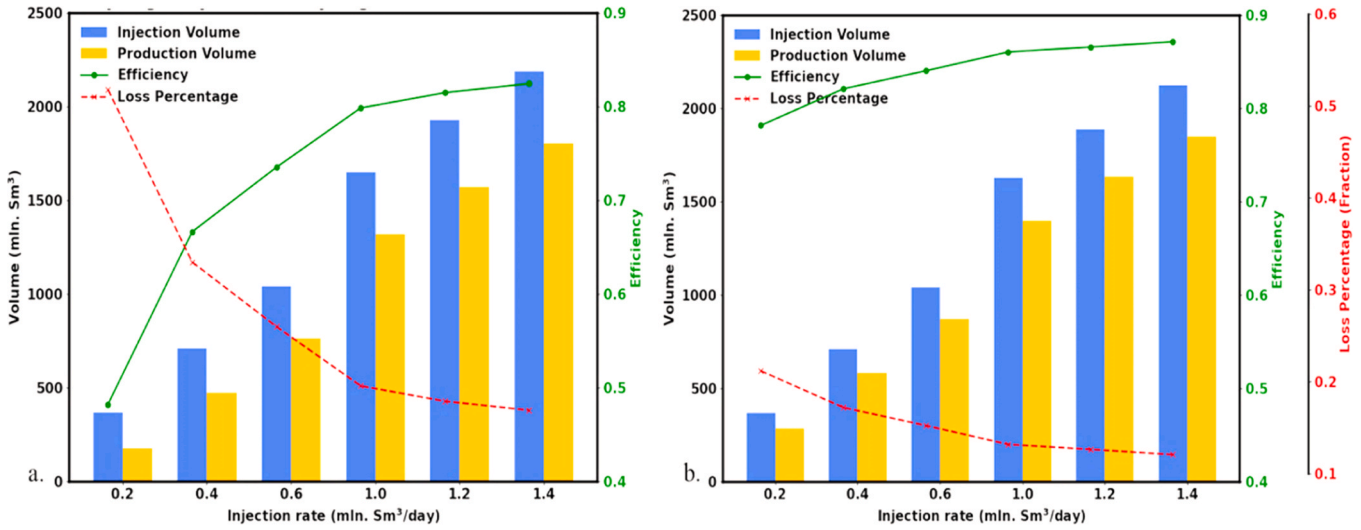

Fig. 11. Efficiency comparison at different injection rates: a) H_2 injection and production in the bottom layer and b) H_2 injection in the bottom layer and production from the top layers.

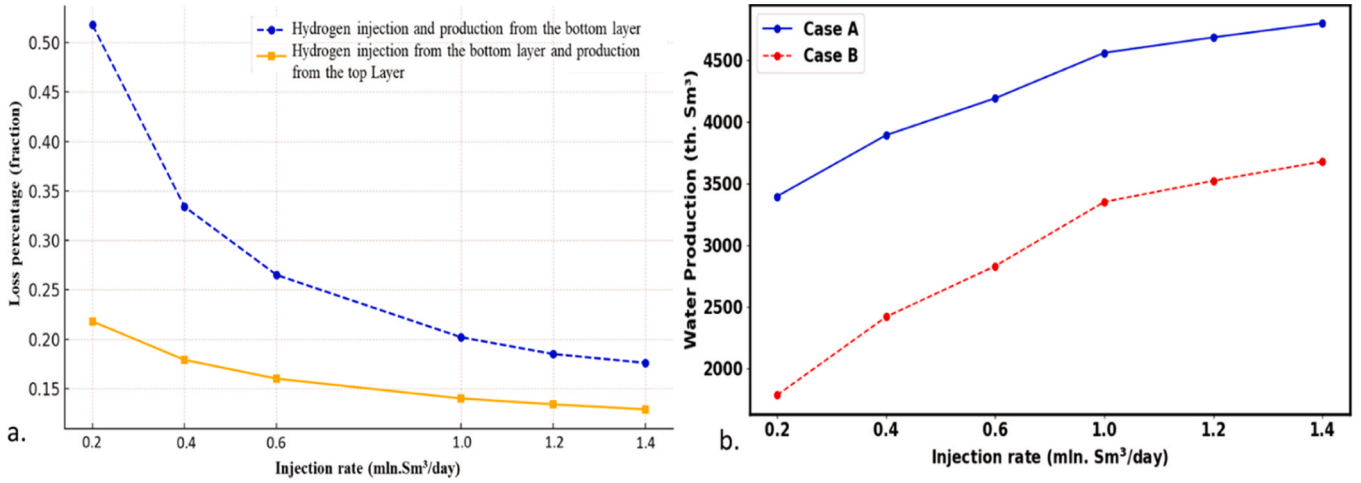

Fig. 12. Injection rate comparison with a) loss percentage (fraction) and b) water production.

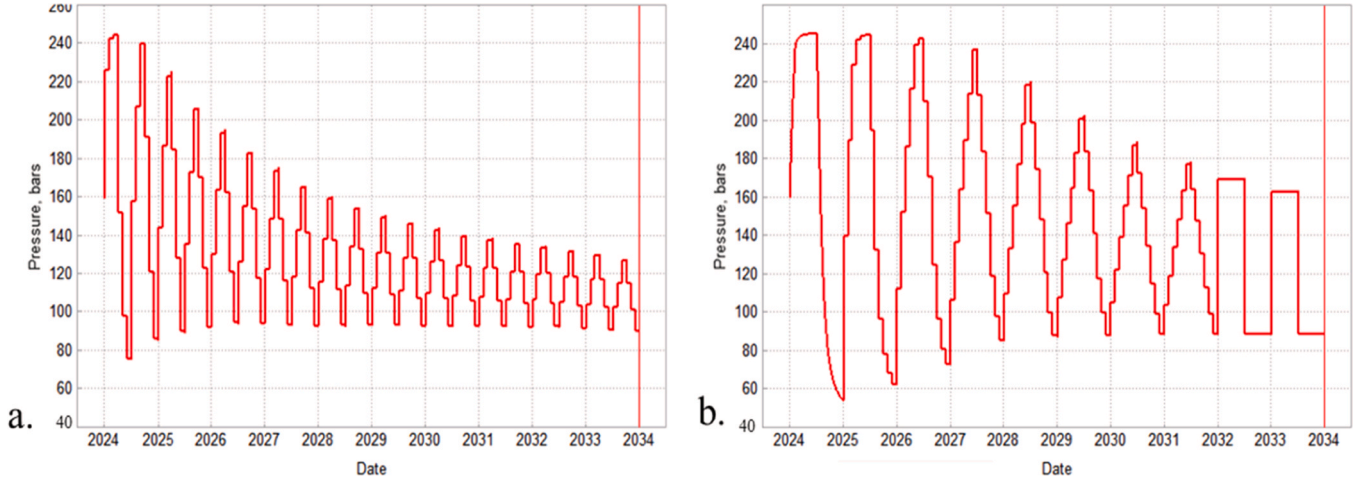

Fig. 13. The pressure variation over time during a) 3-month and b) 6-month injection and production cycle of hydrogen in a saline aquifer.

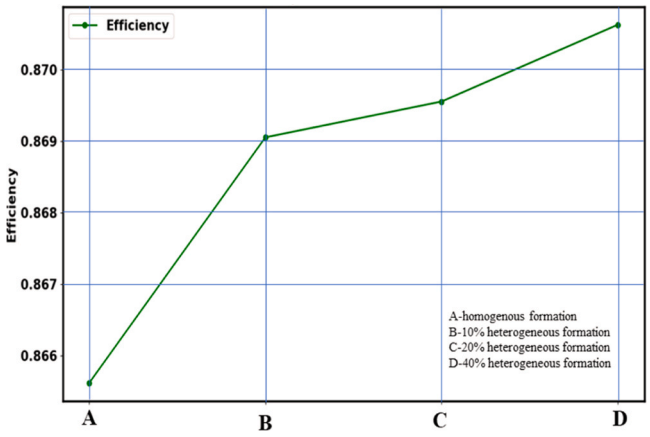

Fig. 14. Impact of reservoir heterogeneity on storage efficiency.

5. Limitation and future scope of the study

The experiments were conducted on a laboratory scale, which may not fully replicate the complexities and scale of actual underground hydrogen storage conditions. The experimental setup was designed to withstand pressures up to 1 bar, significantly lower than those in real underground storage scenarios. The materials used in the experimental setup (fine sand, sandstone, clay, and gravel) may not ideally mimic the properties and behavior of actual subsurface geological formations. In the present study, the simulation model used to replicate laboratory experiments relies on assumptions and limitations, such as the model running at low pressure, being unable to fully replicate what is happening due to pressure and temperature differences, and being based on a 2D grid. The gas produced may contains other gases besides H_2 and may also contains impurities, which were not investigated in this study. The future scope of the study includes extending laboratory-scale experiments to field-scale and developing advanced simulation models to study factors such as wettability, geochemical at pore level, microbial activity, and long-term stability. Also, future work will focus on studying the composition of the gas, specifically identifying, and quantifying any impurities, to gain a more accurate understanding of the hydrogen production process.

6. Conclusions

This study aimed to analyze hydrogen flow behavior and optimize efficiency during UHSP using both experimental and simulation approaches. The laboratory-scale experiment demonstrated promising results, indicating migration through color changes in the BTB dye. CO_2 displaced brine within the sandstone, with preferential flow paths observed in high-permeability layers, and leakage was noted at higher pressures due to tank expansion. The $H_2 + CO_2$ mixture injection demonstrated the effectiveness of porous media for gas storage when combined with an impermeable cap rock. Simulation results indicated that CO_2 initially concentrated near the injection well, forming a confined plume that expanded over time, while the $H_2 + CO_2$ mixture achieved a broader and more uniform distribution, indicating improved displacement efficiency. Optimization scenarios revealed that a 3-month cycle outperformed a 6-month cycle, achieving higher H_2 injection (2128.46 mln. Sm^3) and production volumes (1872.11 mln. Sm^3) with improved efficiency (0.880) and lower loss percentage (12 %). Reducing the observation period from 10 to 5 years resulted in lower efficiency (0.854) and higher water production (5206.02 th. Sm^3). A single-well setup was more efficient (0.880) with reduced losses (256.35 mln. Sm^3) and lower water production (3495.00 th. Sm^3) compared to a two-well configuration. Increasing heterogeneity and optimizing the injection period enhanced gas recovery efficiency, with a 40 % heterogeneous formation and a 3-month injection cycle achieving the highest efficiency (0.882) and the lowest loss percentage (11.8 %). Both experimental and simulation results confirmed the effectiveness of sandstone as a storage medium for gases, with the presence of an impermeable layer being crucial for containment. The simulation provided detailed insights into the dynamic movement and saturation profiles of gases, complementing the experimental observations. The experimental setup highlighted practical challenges, such as leakage due to tank expansion, which were not observed in the simulation. Overall, the study demonstrated the potential for large-scale underground hydrogen storage in geological formations, with both approaches providing valuable insights. The findings suggest optimizing injection cycles, using appropriate cap rocks, and considering reservoir heterogeneity can significantly enhance storage efficiency and safety. Further research is needed to refine these strategies and address practical challenges observed in the experiments. Overall, the study underscores the importance of understanding CO_2 and $H_2 + CO_2$ migration to evaluate reservoir suitability for long-term storage in sandstone formations, which are effective for underground hydrogen storage. Optimization scenarios revealed that shorter injection cycles and increased reservoir heterogeneity enhance storage efficiency.

CRediT authorship contribution statement

Verma Apoorv: Writing-review & editing, writing -original draft, Visualization, Software, Investigation, Methodology, Analysis, Data curation, Conceptualization, Experiment design and execution. **Dangi Shankar Lal:** Experiment execution, Equation Theory Writing, Simulation and Optimization, Visualization. **Malik Shruti:** Writing-review & editing. **Pal Mayur:** Writing-review & editing, Conceptualization, Methodology, Experiment design, Resources, and Supervision.

Funding

The Lithuanian Research Council supported this work through grant no. P-PD-23–090.

Declaration of Competing Interest

Authors declare no conflict of interest.

Acknowledgement

The authors would like to thanks Prof. Brijesh K. Yadav head of the Groundwater Laboratory at the Dept. of Hydrology, Indian Institute of Technology Roorkee, India, for providing access to conduct experiments.

Data availability

Data will be made available on request.

References

Abdellatif, M., Hashemi, M., Azizmohammadi, S., 2023. Large-scale underground hydrogen storage: integrated modeling of reservoir-wellbore system. Int. J. Hydrog. Energy 48 (50), 19160–19171. https://doi.org/10.1016/J.IJHYDENE.2023.01.227.

Akbar, A., Gul, A., Sohail, M., Hedvicakova, M., Haider, S.A., Ahmad, S., Iqbal, S., 2024. Impact of renewable and non-renewable energy resources on CO2 emission: empirical evidence from SAARC. Int. J. Energy Econ. Policy 14 (1), 141–149. https://doi.org/10.32479/IJEEP.15049.

Bahrami, M., Izadi Amiri, E., Zivar, D., Ayatollahi, S., Mahani, H., 2023. Challenges in the simulation of underground hydrogen storage: a review of relative permeability and hysteresis in hydrogen-water system. J. Energy Storage 73, 108886. https://doi.org/10.1016/J.EST.2023.108886.

Berta, M., Dethlefsen, F., Ebert, M., Schäfer, D., Dahmke, A., 2018. Geochemical effects of millimolar hydrogen concentrations in groundwater: an experimental study in the context of subsurface hydrogen storage. Environ. Sci. Technol. 52 (8), 4937–4949. https://doi.org/10.1021/ACS.EST.7B05467.

Boon, M., Hajibeygi, H., 2022. Experimental characterization of > {\text {H}}_2> / water multiphase flow in heterogeneous sandstone rock at the core scale relevant for underground hydrogen storage (UHS). *1*, *12* Sci. Rep. 2022 12 (1), 1–12. https://doi.org/10.1038/s41598-022-18759-8.

Cai, Z., Zhang, K., Guo, C., 2022. Development of a novel simulator for modelling underground hydrogen and gas mixture storage. Int. J. Hydrog. Energy 47 (14), 8929–8942. https://doi.org/10.1016/J.IJHYDENE.2021.12.224.

Chauhan, J. (2018). Transport of CO2 In Porous Media – A Visualisation Study. ⟨https://uis.brage.unit.no/uis-xmlui/handle/11250/2569332⟩.

Dangi, S.L., Karaliūtė, V., Maurya, N.K., Pal, M., 2023. Predicting flow in porous media: a comparison of physics-driven neural network approaches. Math. Models Eng. 9 (2), 52–71. https://doi.org/10.21595/MME.2023.23174.

Dehghani, M.R., Ghazi, S.F., Kazemzadeh, Y., 2024. Interfacial tension and wettability alteration during hydrogen and carbon dioxide storage in depleted gas reservoirs. *1*, *14* Sci. Rep. 2024 14 (1), 1–25. https://doi.org/10.1038/s41598-024-62458-5.

Dodangoda, C., P. G, R., 2024. Quantification of hydrogen depletion and mineral reactivity in underground hydrogen storage reservoirs. Gas Science and Engineering 126, 205318. https://doi.org/10.1016/j.jgsce.2024.205318. ISSN 2949-9089.

Dokhon, W., Goodarzi, S., Alzahrani, H.M., Blunt, M.J., Bijeljic, B., 2024. Pressure decline and gas expansion in underground hydrogen storage: a pore-scale percolation study. Int. J. Hydrog. Energy 86, 261–274. https://doi.org/10.1016/J.IJHYDENE.2024.08.139.

Gao, J., Kong, D., Peng, Y., Zhou, Y., Liu, Y., Zhu, W., 2023. Pore-scale mechanisms and hysteresis effect during multi-cycle injection and production process in underground hydrogen storage reservoir. Energy 283, 129007. https://doi.org/10.1016/J.ENERGY.2023.129007.

Gielen, D., Taibi, E., & Miranda, R. (2019). Hydrogen: A Reviewable Energy Perspective: Report prepared for the 2nd Hydrogen Energy Ministerial Meeting in Tokyo, Japan. ⟨https://www.h2knowledgecentre.com/content/policypaper1305⟩.

Gomez Mendez, I., El-Sayed, W.M.M., Menefee, A.H., & Karpyn, Z.T. (2024). Insights into Underground Hydrogen Storage Challenges: A Review on Hydrodynamic and Biogeochemical Experiments in Porous Media. Energy and Fuels. ⟨https://doi.org/10.1021/ACS.ENERGYFUELS.4C03142/ASSET/IMAGES/LARGE/EF4C03142_0006.JPEG⟩.

Hogeweg, S., Strobel, G., Hagemann, B., 2022a. Benchmark study for the simulation of Underground Hydrogen Storage operations. Comput. Geosci. 26 (6), 1367–1378. https://doi.org/10.1007/S10596-022-10163-5/METRICS.

Hogeweg, S., Strobel, G., Hagemann, B., 2022b. Benchmark study for the simulation of Underground Hydrogen Storage operations. Comput. Geosci. 26 (6), 1367–1378. https://doi.org/10.1007/S10596-022-10163-5/METRICS.

Ichimura, S., Kimura, S., 2019. Present status of pumped hydro storage operations to mitigate renewable energy fluctuations in Japan. Glob. Energy Interconnect. 2 (5), 423–428. https://doi.org/10.1016/J.GLOEI.2019.11.017.

Iglauer, S., Ali, M., Keshavarz, A., 2021. Hydrogen wettability of sandstone reservoirs: implications for hydrogen geo-storage. Geophys. Res. Lett. 48 (3), e2020GL090814. https://doi.org/10.1029/2020GL090814.

Indro, A.P., Sekar, L.K., Matey-Korley, G.V., Ikeokwu, C.C., Okoroafor, E.R., 2024. A compilation of losses related to hydrogen storage in porous media: implications for hydrogen recovery and productivity from saline aquifers. Int. J. Hydrog. Energy 78, 1288–1305. https://doi.org/10.1016/J.IJHYDENE.2024.06.365.

Izadi Amiri, I., Zivar, D., Ayatollahi, S., Mahani, H., 2024. The effect of gas solubility on the selection of cushion gas for underground hydrogen storage in aquifers. J. Energy Storage 80, 110264. https://doi.org/10.1016/J.EST.2023.110264.

Jahanbani Veshareh, M., Thaysen, E.M., Nick, H.M., 2022. Feasibility of hydrogen storage in depleted hydrocarbon chalk reservoirs: assessment of biochemical and chemical effects. Appl. Energy 323, 119575. https://doi.org/10.1016/J.APENERGY.2022.119575.

Jangda, Z., Menke, H., Busch, A., Geiger, S., Bultreys, T., Lewis, H., Singh, K., 2023. Pore-scale visualization of hydrogen storage in a sandstone at subsurface pressure and temperature conditions: trapping, dissolution and wettability. J. Colloid Interface Sci. 629, 316–325. https://doi.org/10.1016/J.JCIS.2022.09.082.

Kolditz, O., Bauer, S., Bilke, L., Böttcher, N., Delfs, J.O., Fischer, T., Görke, U.J., Kalbacher, T., Kosakowski, G., McDermott, C.I., Park, C.H., Radu, F., Rink, K., Shao, H., Shao, H.B., Sun, F., Sun, Y.Y., Singh, A.K., Taron, J., Zehner, B., 2012. OpenGeoSys: an open-source initiative for numerical simulation of thermo-hydro-mechanical/chemical (THM/C) processes in porous media. Environ. Earth Sci. 67 (2), 589–599. https://doi.org/10.1007/S12665-012-1546-X.

Liebscher, A., Wackerl, J., Streibel, M., 2016. Geologic storage of hydrogen – fundamentals, processing, and projects. Hydrog. Sci. Eng. Mater., Process., Syst. Technol. 2, 629–658. https://doi.org/10.1002/9783527674268.CH26.

Liu, G., Smirnov, A.V., 2008. Modeling of carbon sequestration in coal-beds: a variable saturated simulation. Energy Convers. Manag. 49 (10), 2849–2858. https://doi.org/10.1016/J.ENCONMAN.2008.03.007.

Lysyy, M., Ersland, G., Fernø, M., 2022. Pore-scale dynamics for underground porous media hydrogen storage. Adv. Water Resour. 163, 104167. https://doi.org/10.1016/J.ADVWATRES.2022.104167.

Maghami, M.R., Pasupuleti, J., Ekanayake, J., 2024. Energy storage and demand response as hybrid mitigation technique for photovoltaic grid connection: challenges and future trends. J. Energy Storage 88, 111680. https://doi.org/10.1016/J.EST.2024.111680.

Malik, S., Makauskas, P., Karaliūtė, V., Pal, M., Sharma, R., 2024. Assessing the geological storage potential of CO2 in Baltic Basin: a case study of Lithuanian hydrocarbon and deep saline reservoirs. Int. J. Greenh. Gas. Control 133, 104097. https://doi.org/10.1016/J.IJGGC.2024.104097.

Malik, S., Makauskas, P., Sharma, R., Pal, M., 2023. Exploring CO2 storage potential in Lithuanian deep saline aquifers using digital rock volumes: a machine learning guided approach. Adv. Carbon Capture Util. Storage 1 (2), 44–47. https://doi.org/10.21595/ACCUS.2023.23906.

Maury Fernandez, D., Emadi, H., Hussain, A., Thiyagarajan, S.R., 2024. A holistic review on wellbore integrity challenges associated with underground hydrogen storage. Int. J. Hydrog. Energy 57, 240–262. https://doi.org/10.1016/J.IJHYDENE.2023.12.230.

Mubarak, F., Al, Rezaee, R., Wood, D.A., 2024. Economic, societal, and environmental impacts of available energy sources: a review. *Vol. 5, Pages 1232-1265* Eng 2024 5 (3), 1232–1265. https://doi.org/10.3390/ENG5030067.

Najafimarghmaleki, A., Dehghanpour, H., 2024. Evaluating fluid/rock interactions for energy storage in salt caverns: Part I: Brine-rock salt interactions. Energy Fuels. https://doi.org/10.1021/ACS.ENERGYFUELS.4C03271/ASSET/IMAGES/LARGE/EF4C03271_0013.JPEG.

Pan, B., Yin, X., Ju, Y., Iglauer, S., 2021a. Underground hydrogen storage: influencing parameters and future outlook. Adv. Colloid Interface Sci. 294, 102473. https://doi.org/10.1016/J.CIS.2021.102473.

Pan, B., Yin, X., Ju, Y., Iglauer, S., 2021b. Underground hydrogen storage: influencing parameters and future outlook. Adv. Colloid Interface Sci. 294. https://doi.org/10.1016/J.CIS.2021.102473.

Peng, D.Y., Robinson, D.B., 1976. A new two-constant equation of state. Ind. Eng. Chem. Fundam. 15 (1), 59–64. https://doi.org/10.1021/I160057A011/ASSET/I160057A011.FP.PNG_V03.

Perone, G., 2024. The relationship between renewable energy production and CO2 emissions in 27 OECD countries: a panel cointegration and Granger non-causality approach. J. Clean. Prod. 434, 139655. https://doi.org/10.1016/J.JCLEPRO.2023.139655.

Pfeiffer, W.T., Beyer, C., Bauer, S., 2017. Hydrogen storage in a heterogeneous sandstone formation: dimensioning and induced hydraulic effects. Pet. Geosci. 23 (3), 315–326. https://doi.org/10.1144/PETGEO2016-050.

Rahbari, A., Brenkman, J., Hens, R., Ramdin, M., Van Den Broeke, L.J.P., Schoon, R., Henkes, R., Moultos, O.A., Vlugt, T.J.H., 2019. Solubility of water in hydrogen at high pressures: a molecular simulation study. J. Chem. Eng. Data 64 (9), 4103–4115. https://doi.org/10.1021/ACS.JCED.9B00513.

Renné, D.S., 2022. Progress, opportunities and challenges of achieving net-zero emissions and 100% renewables. Sol. Compass 1, 100007. https://doi.org/10.1016/J.SOLCOM.2022.100007.

Saeed, M., Jadhawar, P., 2024. Optimizing underground hydrogen storage in aquifers: the impact of cushion gas type. Int. J. Hydrog. Energy 52, 1537–1549. https://doi.org/10.1016/J.IJHYDENE.2023.08.352.

Schlapbach, L., 2002. Hydrogen as a fuel and its storage for mobility and transport. MRS Bull. 27 (9), 675–679. https://doi.org/10.1557/MRS2002.220.

Shang, Z., Yang, Y., Zhang, L., Sun, H., Zhong, J., Zhang, K., Yao, J., 2024. Hydrogen adsorption and diffusion behavior in kaolinite slit for underground hydrogen storage: a hybrid GCMC-MD simulation study. Chem. Eng. J. 487, 150517. https://doi.org/10.1016/J.CEJ.2024.150517.

Smith, M.E., Stastny, A.L., Lynch, J.A., Yu, Z., Zhang, P., Heineman, W.R., 2020. Indicator dyes and catalytic nanoparticles for irreversible visual hydrogen sensing. Anal. Chem. 92 (15), 10651–10658. https://doi.org/10.1021/ACS.ANALCHEM.0C01769/ASSET/IMAGES/LARGE/AC0C01769_0004.JPEG.

Song, H., Lao, J., Zhang, L., Xie, C., Wang, Y., 2023. Underground hydrogen storage in reservoirs: pore-scale mechanisms and optimization of storage capacity and efficiency. Appl. Energy 337, 120901. https://doi.org/10.1016/J.APENERGY.2023.120901.

Tarkowski, R., 2019. Underground hydrogen storage: characteristics and prospects. Renew. Sustain. Energy Rev. 105, 86–94. https://doi.org/10.1016/J.RSER.2019.01.051.

Tarkowski, R., Uliasz-Misiak, B., 2022. Towards underground hydrogen storage: a review of barriers. Renew. Sustain. Energy Rev. 162, 112451. https://doi.org/10.1016/J.RSER.2022.112451.

Thaysen, E.M., Armitage, T., Slabon, L., Hassanpouryouzband, A., Edlmann, K., 2023. Microbial risk assessment for underground hydrogen storage in porous rocks. Fuel 352, 128852. https://doi.org/10.1016/J.FUEL.2023.128852.

Verma, A., Malik, S., Pal, M., 2025. Evaluating the potential for underground hydrogen storage (UHS) in Lithuania: a review of geological viability and storage integrity. *Vol. 15, Page 1614* Appl. Sci. 2025 15 (3), 1614. https://doi.org/10.3390/APP15031614.

Verma, A., Malik, S., Dangi, S.L., Yadav, B.K., Pal, M., 2024. Hydrogen and CO2 storage in sandstone: understanding porous media behavior. Adv. Carbon Capture Util. Storage 2 (2), 13–16. https://doi.org/10.21595/ACCUS.2024.24675.

Vialle, S., Wolff-Boenisch, D., 2024. Thermodynamic and kinetic considerations of the link between underground hydrogen storage and reductive carbonate dissolution and methane production. Are limestone reservoirs unsuitable for UHS? Chem. Geol. 665, 122304. https://doi.org/10.1016/J.CHEMGEO.2024.122304.

Wallace, J.S., Ward, C.A., 1983. Hydrogen as a fuel. Int. J. Hydrog. Energy 8 (4), 255–268. https://doi.org/10.1016/0360-3199(83)90136-2.

Wang, J., Wu, R., Wei, M., Bai, B., Xie, J., Li, Y., 2023. A comprehensive review of site selection, experiment and numerical simulation for underground hydrogen storage. Gas. Sci. Eng. 118, 205105. https://doi.org/10.1016/J.JGSCE.2023.205105.

Wang, J., Yang, Y., Cai, S., Yao, J., Xie, Q., 2023. Pore-scale modelling on hydrogen transport in porous media: implications for hydrogen storage in saline aquifers. Int. J. Hydrog. Energy 48 (37), 13922–13933. https://doi.org/10.1016/J.IJHYDENE.2022.11.299.

Whitaker, S., 1986. Flow in porous media I: a theoretical derivation of Darcy's law. Transp. Porous Media 1 (1), 3–25. https://doi.org/10.1007/BF01036523/METRICS.
Yang, H., Sun, S., Li, Y., Yang, C., 2018. A scalable fully implicit framework for reservoir simulation on parallel computers. Comput. Methods Appl. Mech. Eng. 330, 334–350. https://doi.org/10.1016/J.CMA.2017.10.016.
Zivar, D., Kumar, S., Foroozesh, J., 2021. Underground hydrogen storage: a comprehensive review. Int. J. Hydrog. Energy 46 (45), 23436–23462. https://doi.org/10.1016/J.IJHYDENE.2020.08.138.